Hindawi
Mathematical Problems in Engineering
Volume 2018, Article ID 8503628, 13 pages
https://doi.org/10.1155/2018/8503628

Research Article

Theoretical and Experimental Analysis of the Hydraulic Actuator Used in the Active Reflector System

Juliang Xiao, Qinyu Liu, Guodong Wang, and Jun Ji

Key Laboratory of Mechanism Theory and Equipment Design of Ministry of Education, Tianjin University, Tianjin 300350, China

Correspondence should be addressed to Juliang Xiao; tjxjl@tju.edu.cn

Received 29 November 2017; Accepted 20 June 2018; Published 26 July 2018

Academic Editor: J.-C. Cortés

In order to improve the control quality of the active reflector system which is used in the 500 m aperture spherical radio telescope (FAST) project, a study on hydraulic actuator is proposed. The dynamic performance of hydraulic actuator is due to the interaction of several physical phenomena. Modeling of such a system needs a unified approach to represent the nonlinear behavior characteristics. Bond graph model is ideal for this task. In addition, conventional PID control strategy cannot achieve the required accuracy and precision, so we combine grey prediction with PID control. Furthermore, a new adjustment mechanism is presented to change the grey step size, which is simple, automatic, less time-consuming, and efficient. Simulations and experiments on the actuator are carried out to evaluate the effectiveness of the proposed control method. In experiments, the velocity error is less than 0.05mm/s and the position error is less than 0.2mm. It shows the actuator meets the astronomical observation requirement totally.

1. Introduction

Five hundred-meter aperture spherical radio telescope (FAST) project belongs to Chinese "megascience" project building in the unique karst area, which will be the largest single aperture radio telescope in the world [1–3]. It is primarily composed of active reflector system, the supporting system, the measurement and control system, and the receiver and the terminal system. As is shown in Figure 1, the fundamental surface of active reflector is with a radius of 300m, caliber of 500m spherical cap surface, whose spherical cap angle is 110 to 120 degrees. In order to realize the active deformation characteristics of radio telescope, the supporting structure of active reflector adopts the cable net structure which consists of ring beam, main cable net, drop-down cable net, triangular reflector unit, hydraulic actuator, and anchor block. The triangular reflector unit is laid in the main cable net which is fixed on the beam, and the triangle vertices are connected by cable net nodes. The drop-down cable net links the hydraulic actuator to each node. In accordance with the angle of celestial bodies (S1 and S2) and the real-time shape of active reflector, hydraulic actuators adjust the triangular reflector units position to form a 300m caliber instantaneous paraboloid in the radio source direction. As a result, electromagnetic waves converge on the focusing surface [4, 5].

In the active reflector system, it requires small installation space, compact volume, large output power, and long-term open-air work of hydraulic actuators. And the hydraulic actuator should mainly realize two working conditions.

Firstly, the actuator changes the observation target, which is the point-to-point motion with a closed-loop velocity control. The average velocity is required to reach 1.6mm/s, and the velocity error is no more than 0.05mm/s. Secondly, the actuator traces the observation target in a closed-loop position control. In this situation, the position error is less than 0.25mm without velocity requirements.

There are two types of hydraulic actuators: valve-controlled cylinder [6–8] and pump-controlled cylinder [9, 10]. The valve-controlled hydraulic actuator with hydraulic servo valve as control unit is gradually replaced by the pump-controlled hydraulic actuator because of its characteristics of large throttling loss, low efficiency, high requirement of oil cleanliness, and high price. Therefore, based on the above requirements, the hydraulic actuator with the form of pump-controlled differential cylinder is adopted in this paper. The

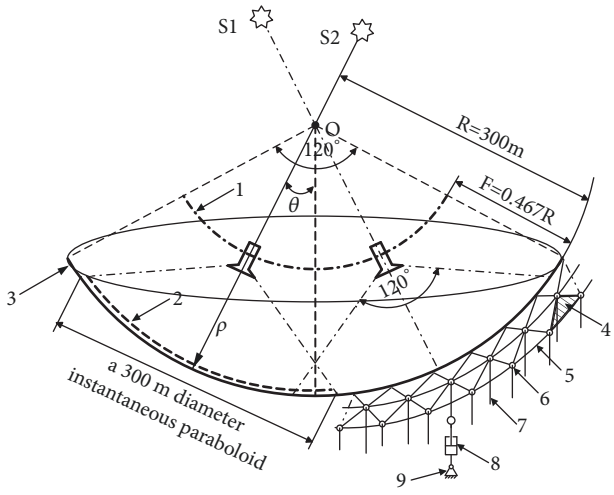

Figure 1: The optical principle diagram of the active reflector system. 1: focusing surface; 2: paraboloid; 3: spherical surface; 4: triangular reflector unit; 5: main cable net; 6: cable net node; 7: drop-down cable net; 8: hydraulic actuator; 9: anchor block.

hydraulic actuators mentioned in this paper are all these kinds of hydraulic actuators.

The recent research on pump-controlled differential cylinder mainly focuses on two aspects of modeling and control strategy.

For modeling, in [11], the AMESim software is directly used to model the whole hydraulic system, rather than focusing on the mathematical description of the system model. In [12], a mathematical model of the hydraulic system is established by state space equations, but its research point is the nonlinearity of friction force, and the mathematical model is relatively simple. In this paper, the hydraulic actuator system is modeled with the method of bond graph, which not only considers the flow compensation due to the asymmetry of hydraulic cylinder, but also takes the coupling of several energy domains into account. A precise mathematical model of the hydraulic actuator is established effectively.

For the control strategy, in [13, 14], the nonlinear dynamic feedforward compensation control strategy on the basis of reforming the flow distribution principle of the pump or using a special asymmetrical pump is proposed to improve the dynamic and static performance of the differential cylinder. In [15, 16], sliding mode control and robust H∞ sliding mode control are developed, which can achieve accurate trajectory tracking and effectively resist external interference, but the control object is the reformed single-rod cylinder, not the differential cylinder. Moreover, the control signal of sliding mode control cannot avoid the chattering, which would damage the mechanical system. In [17, 18], the neural network is used as an identifier or a controller to the pump-controlled differential cylinder system to accelerate the convergence rate of the tracking error. However, after each operation, the weights of the neural network need to be updated; such complicated calculations make it unsuitable for engineering practice. In this paper, a switching grey prediction PID control strategy is proposed, which is not based on any modification of system components. Besides, the interaction of several physical phenomena, the uncertainty of the system parameters, the hysteresis, and other nonlinear factors are considered comprehensively. Grey system theory is particularly designed for handling situations in which only limited data are available, especially as the system is not well-defined and fully understood. The grey prediction technique has been successfully employed to solve many engineering problems including robot position control, piezo-actuators position control which has the inherent hysteresis characteristic, a nonlinear liquid level system control, and boiler drum level control [19–22]. Therefore, the goal of this control strategy is to apply grey theory to tune up the control parameters. Moreover, this paper describes a simpler scheme to change the step size of the grey predictor, which not only avoids the complexity that the step size is changed by the establishment of fuzzy rules [23], but also avoids the inaccuracy that the step size is changed by step transform threshold set by experience [24].

In this paper, the working principle and the integrated structure of hydraulic actuator are designed for FAST project. Secondly, its state space model is established by the method of bond graph. Then, a switching grey prediction PID control strategy is designed according to the working conditions of the hydraulic actuator in the active reflector system. In order to verify the effectiveness of the whole control strategy, not only is simulation carried out on the basis of the bond graph model, but also a field experiment platform is built in FAST and field tests are conducted.

2. Hydraulic System of the Actuator

The hydraulic system is in the form of pump-controlled hydraulic differential cylinder, whose working principle is showed in Figure 2 [25]. Apparently, the unique system could not only meet the movement requirements of active reflector system just by controlling the rod chamber of differential hydraulic cylinder, but also allow a variable transmission of power by connecting a pump directly to an actuator [26].

2.1. Working Principle of Installation and Commissioning

2.1.1. Automatic Adjustment. In this case, there is no-load. As the piston rod extends out, the solenoid valves (DC1 and DC2) are energized and the motor is reversed (counterclockwise), so the rod chamber is connected to the nonrod chamber. The oil supplied by the pump is combined with the oil from rod chamber and then flows into the nonrod chamber to realize the output of the piston rod by using differential output structure.

When the piston rod is retracted, DC1 and DC2 are off, while the motor is also reversed. The oil flows from the oil tank to the rod chamber, passing through the pump and YDF. Oil in nonrod chamber flows back to the oil tank.

2.1.2. Manual Adjustment. In the absence of electricity, the piston rod can be extended or retracted at a certain speed

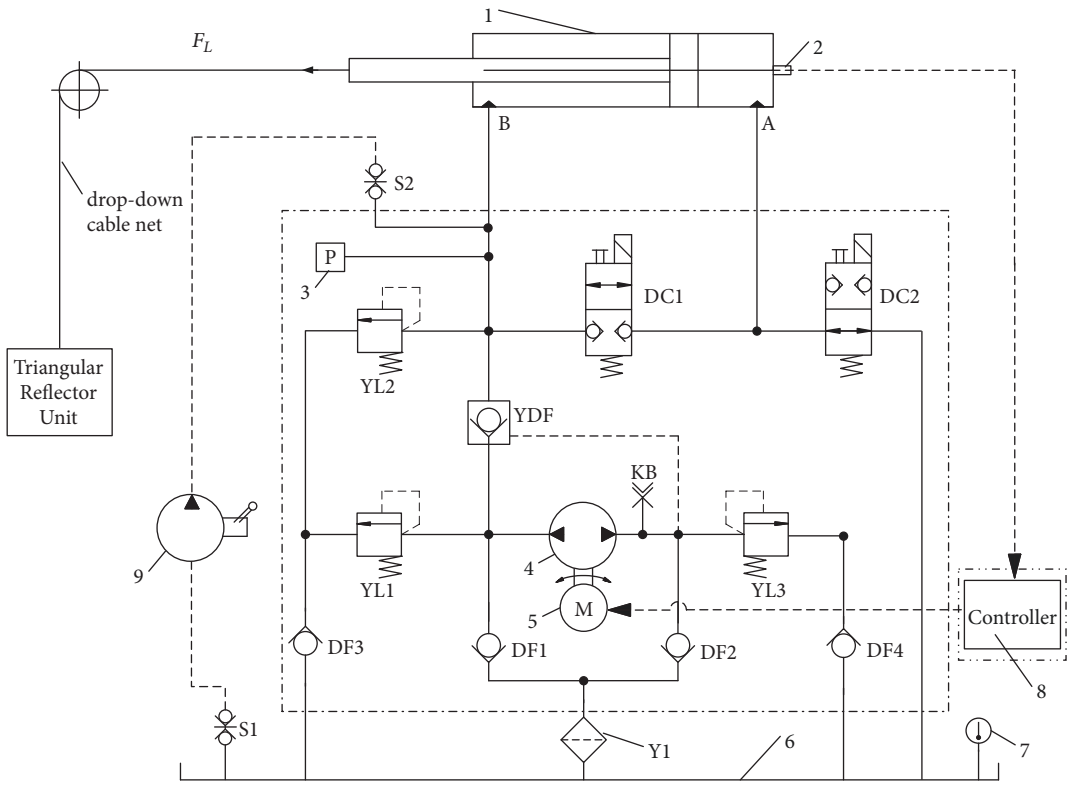

Figure 2: The hydraulic schematic diagram of hydraulic actuator. 1: hydraulic differential cylinder; 2: displacement sensor; 3: pressure sensor; 4: bidirectional quantitative gear pump; 5: two-phase hybrid stepping motor; 6: oil tank; 7: temperature sensor; 8: electric control system; 9: hand pump; DC1 and DC2: solenoid valves; YL1: relief valve; YL2: overflow valve; YL3: counterbalance valve; YDF: pilot operated check valve; DF1, DF2, DF3, and DF4: check valves; S1 and S2: quick-change connector; KB: pressure joints; Y1: filter.

to meet the commissioning needs by using quick-change connector and hand pump.

2.2. Working State. In this case, the actuator is pulled by the triangular reflector unit, solenoid valves (DC1 and DC2) are off all the time, and the nonrod chamber is connected to the tank. When the piston rod extends out, the external load is driving force. On the contrary, the external load is resistance when the piston is retracted. The system can realize the automatic correction and compensation in a closed-loop control condition, while the velocity and position signals of the piston rod are fed back to the electrical control system through the sensor.

As the piston rod extends out, the motor is clockwise, and the outlet pressure of the gear pump is increasing. When the pressure reaches the set pressure of YL3, the YDF opens. With the external load, the oil flows from the rod chamber to the nonrod chamber via the YDF, gear pump, and YL3. Because the two chamber areas are different, the compensatory oil flowing into the nonrod chamber is from the tank.

When the piston is retracted, the motor is reversed, the oil is transported to the rod chamber by the gear pump, and the oil in nonrod chamber flows back to the tank.

2.3. Integrated Structure. The mechanical structure of hydraulic actuator is shown in Figure 3. The integrated valve block consists of solenoid valve, relief valve, overflow valve, counterbalance valve, pilot operated check valve, check valves, filter, quick-change connector, power supply, and communication interface, which not only optimizes the layout of the components, but also saves the volume. The switch power supply is a low voltage DC, and the electric protective cover is made of die cast aluminum. To effectively restrain the temperature rise, the heat conducting pipes are arranged on the electric machine to carry out auxiliary heat radiation.

The hydraulic actuator does not require extra equipment, such as oil pipelines and large external control system. Electrical control part is arranged in the motor terminal support, and the displacement sensor mounted on the cylinder bottom feeds back position signal to the controller. In addition, sealing structure makes the oil avoid the external pollution and improves the adaptability of the actuator.

2.4. System Block Diagram. System block diagram is illustrated in Figure 4, which can also be called the hardware flow chart of the closed-loop control system. In normal working condition, external power supply provides electricity for system by the filter installed in the hydraulic actuator; external control signal is delivered to control port by fiber interface. Closed-loop control of the hydraulic system is implemented by the displacement sensor, while the temperature signal and

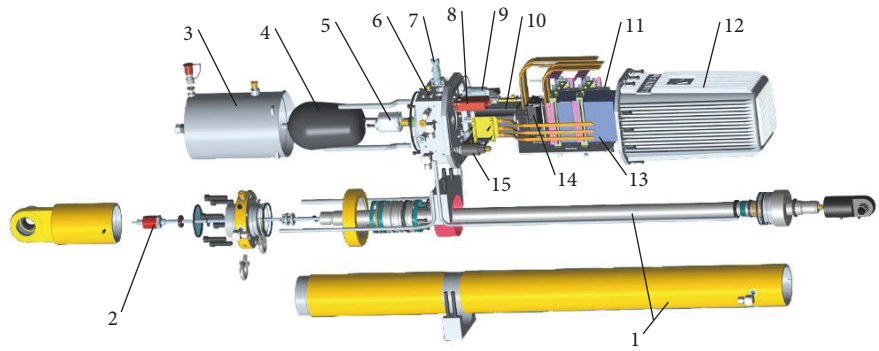

Figure 3: Hydraulic actuator structure. 1: hydraulic differential cylinder; 2: displacement sensor; 3: oil tank; 4: air float; 5: gear pump; 6: integrated valve block; 7: power interface; 8: wave filter; 9: temperature and pressure sensor; 10: two-phase hybrid stepping motor; 11: controller; 12: electric protective cover; 13: switching power supply; 14: motor driver; 15: solenoid valve.

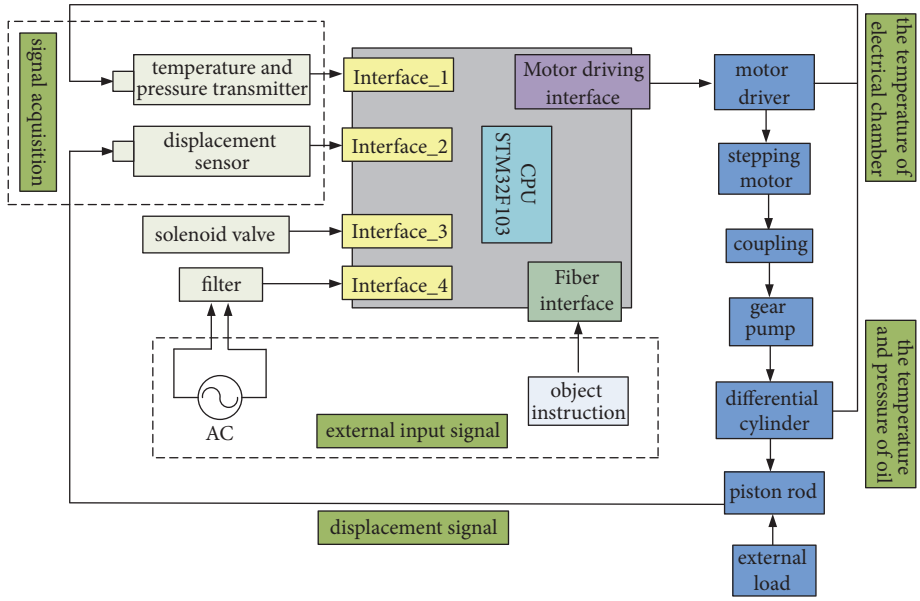

Figure 4: System block diagram.

pressure signal are just regarded as warning signals to ensure the security of the system.

3. Dynamic Bond Graph Model of the System

Modeling an actuator system is a complex process. The reasons are as follows.

First of all, the hydraulic actuator is a nonlinear and uncertain system due to the asymmetry of differential cylinder and the influence of environmental temperature on the hydraulic fluid bulk modulus and the hysteresis [27]. Secondly, the hydraulic actuator system has the coupling of several energy domains (mechanical, electrical, hydrodynamic, etc.) [28–31]. Moreover, traditional modeling methods such as transfer functions cannot meet the requirements of modeling a multi-input system. Finally, for this hydraulic actuator, six state variables need to be selected while modeling by the state equations directly. However, the selection of so many state variables is very difficult. Hence, the bond graph approach is proposed which can decompose the system into subsystems to exchange energy. The global state space equation can be established accurately by this method.

In the bond graph, 0-Junction is a common effort junction which relates effort variables at one point; 1-Junction is a common flow junction which relates flow variables at one point. *TF* is a converter which describes a transformation relationship between two effort variables or two flow variables in the process of energy transfer. *GY* is a gyrator which describes a transformation relationship between effort variables and flow variables in the process of energy transfer.

The system's main power flows are shown in Figure 5.

3.1. Bond Graph Model of the Stepping Motor. Essentially, two-phase hybrid stepping motor is low speed salient pole

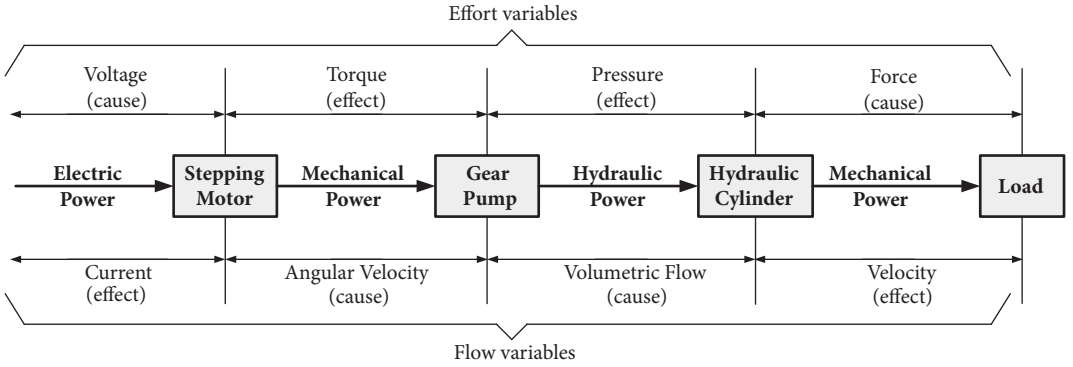

Figure 5: The power flows.

permanent magnet synchronous motor. Therefore, the design of the hybrid stepping motor servo system can consult with the experience of the permanent magnet synchronous servo system [32, 33].

The voltage balance equation is shown as follows:

$$U_A = Ri_A + L\frac{di_A}{dt} - z_r\Phi_m\omega_e \sin\left(z_r\theta_r\right)$$
$$U_B = Ri_B + L\frac{di_B}{dt} + z_r\Phi_m\omega_e \cos\left(z_r\theta_r\right) \quad (1)$$

where U_A and U_B represent the stator voltage of A axis and B axis, respectively, R is the winding resistance, L is the inductance coefficient of winding, i_A and i_B are the current in winding, z_r is the rotor teeth number, Φ_m is the magnetic flux of permanent magnet, ω_e is the electric angular velocity of the rotor, and θ_r is the angular displacement of the rotor.

The electromagnetic torque equation is

$$T_e = -z_r\Phi_m i_A \sin\left(z_r\theta_r\right) + z_r\Phi_m i_B \cos\left(z_r\theta_r\right) \quad (2)$$

The mechanical motion equation is

$$T_e = J_m\frac{d^2\theta_r}{dt^2} + B_m\frac{d\theta_r}{dt} + T_L \quad (3)$$

where T_L is the load torque, J_m is the moment of inertia of the rotor, B_m is the viscous friction coefficient.

The bond graph of the motor with the electrical loss and mechanical loss into consideration is shown in Figure 6, where $MSe1$ is the effort variable on the input port, R_f is the internal resistance caused by the viscous friction of the motor (i.e., $R_f = 1/\mathrm{B}_m$), k_e is the torque coefficient (i.e., $k_e = z_r\Phi_m$), T_{out} is the output torque, and ω_{out} is the output speed.

3.2. Bond Graph Model of the External Gear Pump. The diagram of gear pump is shown in Figure 7.

Define n as the rotation speed of the pump and V_t as the displacement of the pump. p_{in}, Q_{in}, p_{out}, and Q_{out} are the pressure and flow of the pump inlet and outlet, respectively, and Δp is the pressure difference.

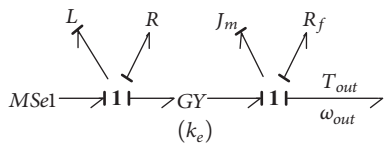

Figure 6: The model of two-phase hybrid stepping motor.

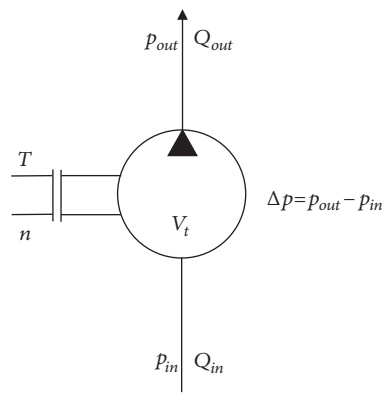

Figure 7: The diagram of gear pump.

The flow equation of gear pump is

$$Q = nV_t - Z_v\Delta p - C_v\frac{d\left(\Delta p\right)}{dt}$$
$$Z_v = \left|\frac{\partial Q}{\partial\left(\Delta p\right)}\right| \quad (4)$$

where Z_v is the internal leakage coefficient; C_v is the liquid capacity of the pump working chamber.

The torque equation of gear pump is

$$T = \left(k_3{}' + \frac{V_t}{2\pi}\right)\Delta p - b_n n - 2\pi J_P\frac{dn}{dt}$$
$$b_n = \frac{\partial T}{\partial n} \quad (5)$$

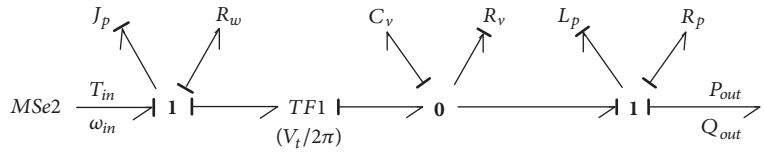

Figure 8: The model of external gear pump.

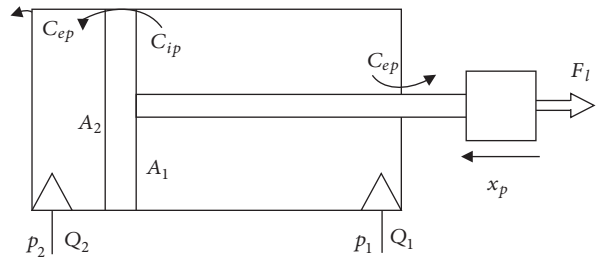

Figure 9: The diagram of hydraulic differential cylinder.

where $k_3{}'$ is the torque loss coefficient because of the pressure, b_n is the linearization coefficient, and J_P is the moment of inertia of the pump.

According to the equivalent of hydraulic power and mechanical power, the linear motion equation of pump can be obtained:

$$\Delta p_p = K_p \Delta p - R_p Q_t - L_p \frac{dQ_t}{dt} \tag{6}$$

where Δp_p is the actual pressure difference during the pump working, $K_p = 2\pi k_3/V_t$, $k_3 = k_3{}' + V_t/2\pi$, $R_p = 2\pi b_n/V_t{}^2$, $L_p = J_p \cdot (2\pi/V_t)^2$, and Q_t is theoretical flow (i.e., $Q_t = nV_t$).

The bond graph of the external gear pump is established based on the above equations, which is shown in Figure 8. In this model, $MSe2$ is the effort variable on the input port of the gear pump; T_{in} is the input torque; ω_{in} is the input angular velocity; P_{out} is the output pressure; Q_{out} is the output flow rate. R_w is internal resistance caused by rotational resistance loss of the pump, R_v is internal resistance caused by internal leakage of the pump (i.e., $R_v = 1/Z_v$).

3.3. Bond Graph Model of the Hydraulic Cylinder. The schematic diagram of hydraulic differential cylinder is shown in Figure 9.

Considering the compressibility of the hydraulic fluid and leakage in the hydraulic differential cylinder, the flow equation can be obtained:

$$\begin{aligned} Q_1 &= A_1 \dot{x}_p + C_{ip}(p_1 - p_2) + C_{ep} p_1 + \frac{V_1}{\beta_e}\frac{dp_1}{dt} \\ Q_2 &= A_2 \dot{x}_p + C_{ip}(p_1 - p_2) - C_{ep} p_1 - \frac{V_2}{\beta_e}\frac{dp_2}{dt} \end{aligned} \tag{7}$$

where Q_1 and Q_2 are the flow of the rod chamber and nonrod chamber; p_1, A_1 and p_2, A_2 are the pressure and effective area of the rod chamber and nonrod chamber, respectively. C_{ip}, C_{ep} are the internal leakage coefficient and external leakage coefficient of the cylinder. V_1 and V_2 are the liquid volume of the rod chamber and nonrod chamber. β_e is the bulk modulus of hydraulic fluid; x_p is the displacement of the piston rod. The pressure of nonrod chamber is close to zero because it is connected to the tank all the time, so we define that $p_2 = 0$. Assuming that the initial volume of rod chamber is zero, L_s is the stroke of hydraulic cylinder, and V_1, V_2 can be simplified to

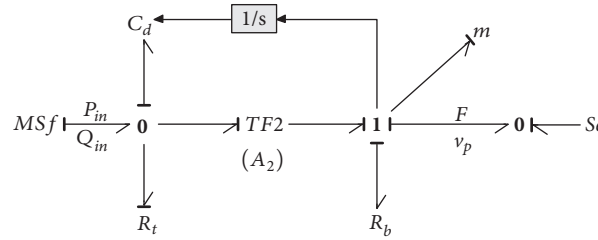

Figure 10: The model of hydraulic differential cylinder.

$$\begin{aligned} V_1 &= A_1 x_p \\ V_2 &= A_2 \left(L_s - x_p\right) \end{aligned} \tag{8}$$

The force balance equation of the hydraulic cylinder is

$$p_1 A_1 - p_2 A_2 = m\ddot{x}_p + B_b \dot{x}_p + F_l \tag{9}$$

where m is the total mass which consists of the piston mass and the reduced mass delivered by the load, B_b is the total viscous damping coefficient, and F_l is the pull of the cable net.

From the above equations, we can get the bond graph of the hydraulic cylinder, which is shown in Figure 10.

In the model of hydraulic cylinder, MSf is the input flow variable; P_{in} is the input pressure; Q_{in} is the input flow; F is the output force; v_p is the output velocity. Se is force source, which is the pull of the cable net. R_b is internal resistance caused by viscous damping (i.e., $R_b = 1/B_b$); R_t is internal resistance

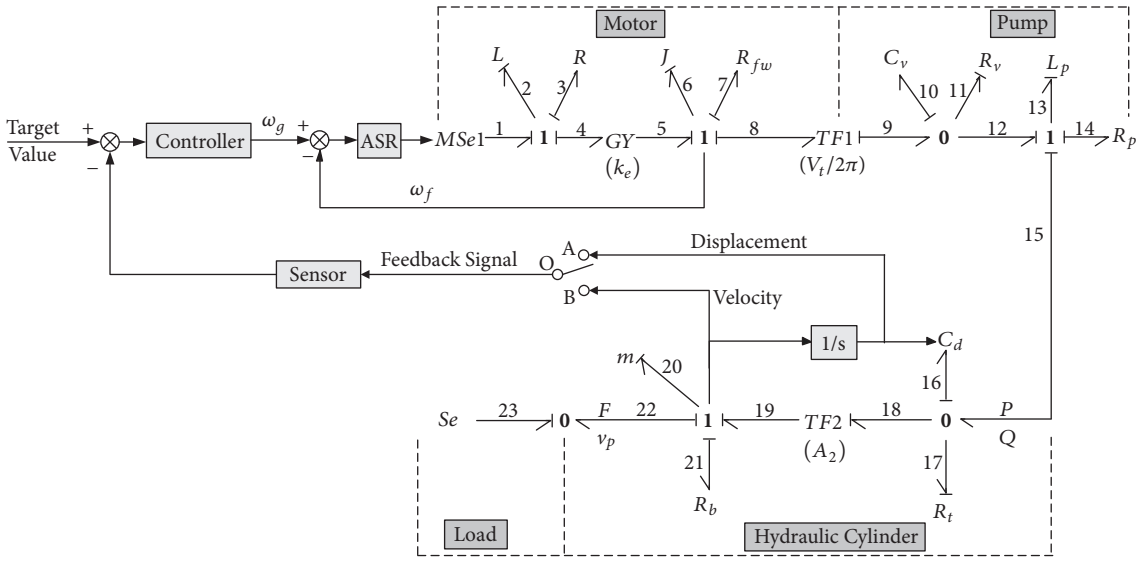

Figure 11: Closed-loop control system model of hydraulic actuator.

caused by the internal leakage and external leakage of the cylinder (i.e., $R_t = 1/(C_{ip} + C_{ep})$). C_d is the liquid capacity of the rod chamber. When the piston rod is at the midpoint of the hydraulic cylinder, the stability was worst, so we compute liquid capacity based on midpoint. The liquid capacity $C_d(t)$ of the rod chamber at the time t is

$$C_d(t) = \frac{\left(A_1 \cdot L_s/2 - A_1 \cdot \int v_p(t)\,dt\right)}{\beta_e} \tag{10}$$

3.4. Global System Modeling. In summary, the bond graph model of the system can be integrated into the form which is shown in Figure 11, where J is the total moment of inertia of the motor rotor and the pump; R_{fw} is the total resistance loss coefficient of motor and pump. The voltage of the motor $MSe1$ is controlled by the automatic speed regulator (ASR), while the essence of ASR is the PI regulator whose input is the difference value of target angular velocity and output angular velocity. According to the principle of stepping motor, the following equation shows the relationship between the pulse frequency and the angular displacement:

$$\theta_i(t) = K_\theta \cdot \int f(t)\,dt \tag{11}$$

where $f(t)$ represents the pulse frequency function and K_θ represents the step angle of the stepping motor. Therefore, we can control the angular displacement and the rotation velocity of stepping motor by controlling $f(t)$.

3.5. State Equation Expression of the System. The system is multiple input single output system, which contains six energy storage elements. Two inputs are, respectively, $MSe1$ and Se; the output is v_p. According to the characteristic equation of every energy storage element and the constraint equation of each node, mathematical equation can be established as follows:

$$\begin{aligned}
\dot{P}_2 &= MSe1 - \frac{R}{L}P_2 - \frac{k_e}{J}P_6 \\
\dot{P}_6 &= \frac{k_e}{L}P_2 - \frac{R_{fw}}{J}P_6 - \frac{V_t}{2\pi C_v}V_{10} \\
\dot{V}_{10} &= \frac{V_t}{2\pi J}P_6 - \frac{1}{C_v R_v}V_{10} - \frac{1}{L_p}P_{13} \\
\dot{P}_{13} &= \frac{1}{C_v}V_{10} - \frac{R_p}{L_p}P_{13} - \frac{1}{C_d}V_{16} \\
\dot{V}_{16} &= \frac{1}{L_p}P_{13} - \frac{1}{C_d R_t}V_{16} - \frac{A_2}{m}P_{20} \\
\dot{P}_{20} &= \frac{A_2}{C_d}V_{16} - \frac{R_b}{m}P_{20} - Se
\end{aligned} \tag{12}$$

The 6 state variables are, respectively, the generalized momentum P_2 at bond 2, the generalized momentum P_6 at bond 6, the generalized displacement V_{10} at bond 10, the generalized momentum P_{13} at bond 13, the generalized displacement V_{16} at bond 16, and the generalized momentum P_{20} at bond 20.

The state space expression of the system is

$$\begin{aligned}
\dot{X}(t) &= A(t) \cdot X(t) + B(t) \cdot U(t) \\
Y(t) &= C(t) \cdot X(t) + D(t) \cdot U(t)
\end{aligned} \tag{13}$$

where $X(t) = \begin{bmatrix} P_2 & P_6 & P_{13} & P_{20} & V_{10} & V_{16} \end{bmatrix}^T$ is state variable, $U(t) = \begin{bmatrix} MSe1 & Se \end{bmatrix}^T$ is input variable, and $Y(t) = [v_p]$ is output variable.

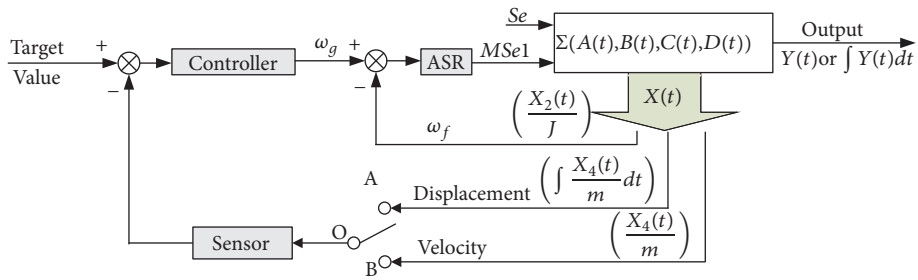

Figure 12: Computer simulation model of hydraulic actuator.

In the system, the state matrix $A(t)$, input matrix $B(t)$, the output matrix $C(t)$, and direct coupling matrix $D(t)$ are

$$A(t) = \begin{bmatrix} -\frac{R}{L} & -\frac{k_e}{J} & 0 & 0 & 0 & 0 \\ \frac{k_e}{L} & -\frac{R_{fw}}{J} & 0 & 0 & -\frac{V_t}{2\pi C_v} & 0 \\ 0 & 0 & -\frac{R_p}{L_p} & 0 & \frac{1}{C_v} & -\frac{1}{C_d} \\ 0 & 0 & 0 & -\frac{R_b}{m} & 0 & \frac{A_2}{C_d} \\ 0 & \frac{V_t}{2\pi J} & -\frac{1}{L_p} & 0 & -\frac{1}{C_v R_v} & 0 \\ 0 & 0 & \frac{1}{L_p} & -\frac{A_2}{m} & 0 & -\frac{1}{C_d R_t} \end{bmatrix} \quad (14)$$

$$B(t) = \begin{bmatrix} 1 & 0 & 0 & 0 & 0 & 0 \\ 0 & 0 & 0 & -1 & 0 & 0 \end{bmatrix}^T$$

$$C(t) = \begin{bmatrix} 0 & 0 & 0 & \frac{1}{m} & 0 & 0 \end{bmatrix}$$

$$D(t) = 0$$

As a result, the global system modeling of the closed-loop system can be expressed as in Figure 12, which is simple and convenient.

4. System Controller

4.1. Schematic of Switching Grey Prediction PID Control. As showed in Figure 13, the control principle of the switching grey prediction PID (SGPID) control is achieved through adding the grey prediction model into the feedback loop of PID controller.

If $Y^{(0)}(t)$ is the sampling value at time t, the equal-dimensional new information sequence composed of the most recent n data is described by

$$Y^{(0)} = \left(Y^{(0)}(t-n+1), Y^{(0)}(t-n+2), \cdots, Y^{(0)}(t)\right) \quad (15)$$

According to the metabolic principle, the equal dimension new information GM (1, 1) model is constructed [34]. The m step forecasting output of the system is

$$\widehat{Y}^{(0)}(t+m) = \left[Y^{(0)}(t-n+1) - \frac{b}{a}\right]\left(1-e^{a}\right)e^{-a(t+m-1)} \quad (16)$$

where a and b are the development coefficient and the grey input coefficient; m is the forecasting step size. In industrial control, the dimension of the sequence for constructing equal-dimensional new information GM (1, 1) model is not too large, usually $n = 5$.

The forecasting step size m has a prominent impact on the control effect of the grey prediction PID control system. In order to improve the performance of the controller further, a new step adjustment mechanism is introduced to change the step size of the grey predictor. It can adjust the step size automatically according to the prediction error $e(t)$, the actual error $E(t)$, and the rate of actual error change $EC(t)$.

4.2. Step Adjustment Mechanism (SAM). As showed in Table 1, if $e(t) \cdot E(t) < 0$, it indicates that the output of the system is close to the set value; thus the absolute value of the forecasting step should be a smaller value in order to avoid overshoot. On the contrary, when $e(t) \cdot E(t) \geq 0$, it shows that the output is seriously deviated from the set value, and the actual error is large, so the absolute value of the forecasting step should be a larger value.

5. Simulation and Analysis

In order to verify the effectiveness of the whole control strategy, the simulation is carried out using MATLAB software. The global state space equation obtained by bond graph is adopted as the system mathematical model in the simulation. Assuming that the initial position of the piston rod is at the midpoint of the hydraulic cylinder, when the piston rod extends out, the displacement is the positive. The quality of the triangular reflector unit is 7000kg, the displacement of the gear pump is $1.0 \times 10^{-6}\mathrm{m}^3/\mathrm{r}$, the diameter of piston rod is 60mm, the diameter of hydraulic cylinder is 100mm, and the stroke of hydraulic cylinder is 1200mm.

Table 1: Step adjustment strategy.

$EC(t)$	The judgment criterion	$E(t)$	Control Mode	m
$EC(t) < 0$: the response of the system is in the rising phase.	$e(t) \cdot E(t) < 0$: the output is close to the target.	$E(t) \geq 0$: the output is close to the target.	rise slowly to avoid overshoot	1
		$E(t) < 0$: the output slightly exceeds the target.	restrain overshoot	2
	$e(t) \cdot E(t) \geq 0$: the output is seriously deviated from the target.	$E(t) \geq 0$: the output is greatly lower than the target.	rise rapidly to reduce rise time	-2
		$E(t) < 0$: the output greatly exceeds the target.	down rapidly	3
$EC(t) > 0$: the response of the system is in the decline phase.	$e(t) \cdot E(t) < 0$: the output is close to the target.	$E(t) \geq 0$: the output slightly exceeds the target.	restrain overshoot	2
		$E(t) < 0$: the output is close to the target.	down slowly to avoid overshoot	1
	$e(t) \cdot E(t) \geq 0$: the output is seriously deviated from the target.	$E(t) \geq 0$: the output greatly exceeds the target.	rise rapidly	3
		$E(t) < 0$: the output is greatly lower than the target.	down rapidly to reduce fall time	-2
$EC(t) = 0$: the response of the system is in the stationary phase.	–	Constant	keep steady to avoid the static error and oscillation	1

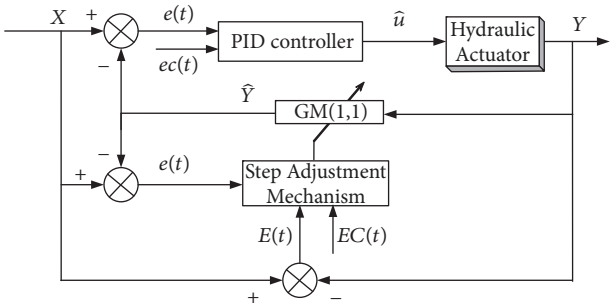

Figure 13: The schematic diagram of SGPID.

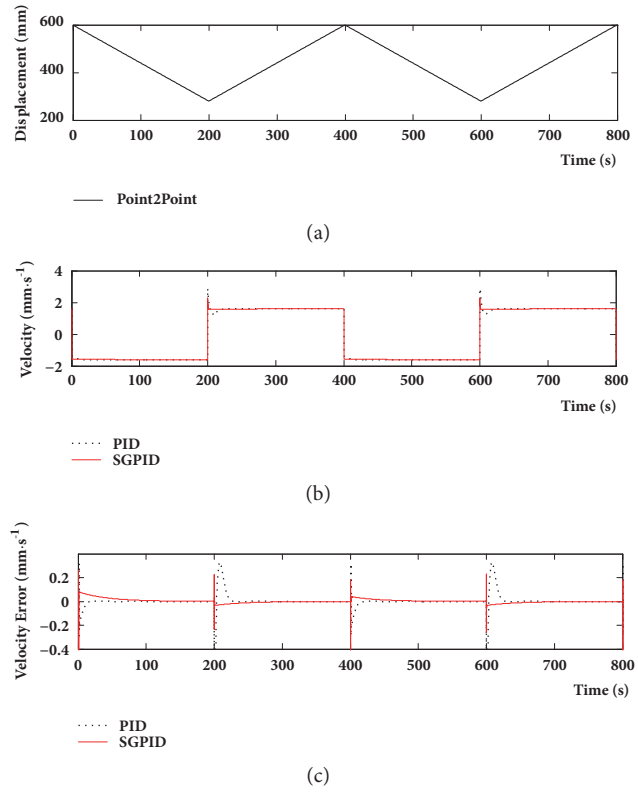

Figure 14: Simulation of changing the source condition.

5.1. Simulation of Changing the Target Source. In this condition, the switch OB in Figure 11 switches on to realize the velocity closed-loop control of the system. In order to achieve the point-to-point changing source movement of the piston rod and make piston rod move between 280mm and 600mm, the square wave signal whose amplitude is 1.6mm/s and period is 400s is given to the system to simulate two kinds of state of velocity signal (i.e., −1.6mm/s and +1.6mm/s). The displacement of piston rod is shown in Figure 14(a).

Two different strategies are simulated under the same control parameters ($K_p = 2.26$, $K_i = 0.95$, and $K_d = 0.16$). With the PID control strategy and the SGPID control strategy applied to the hydraulic system, the velocity curve and the velocity error curve are separately given in Figures 14(b) and 14(c).

When the piston rod is retracted from 600mm to 280mm at a speed of −1.6mm/s, two kinds of control strategies can maintain velocity response without oscillation. However, the velocity controlled by PID strategy appears with apparent delay; in other words, response time is longer, and its velocity error is less than 0.2mm/s. On the contrary, SGPID strategy has a quick response and the velocity error has reduced to less than 0.048mm/s.

As the piston rod extends out from 280mm to 600mm at a speed of +1.6mm/s, the velocity controlled by PID strategy appears with obvious oscillation and overshoot, and

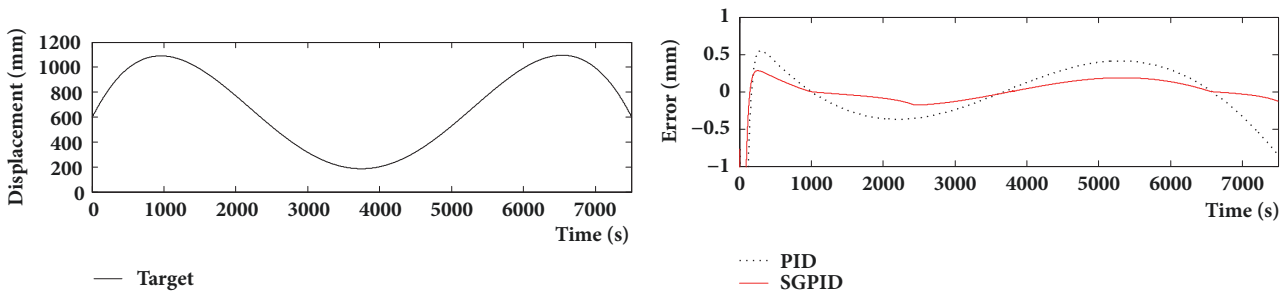

Figure 15: Simulation of the scanning tracking condition.

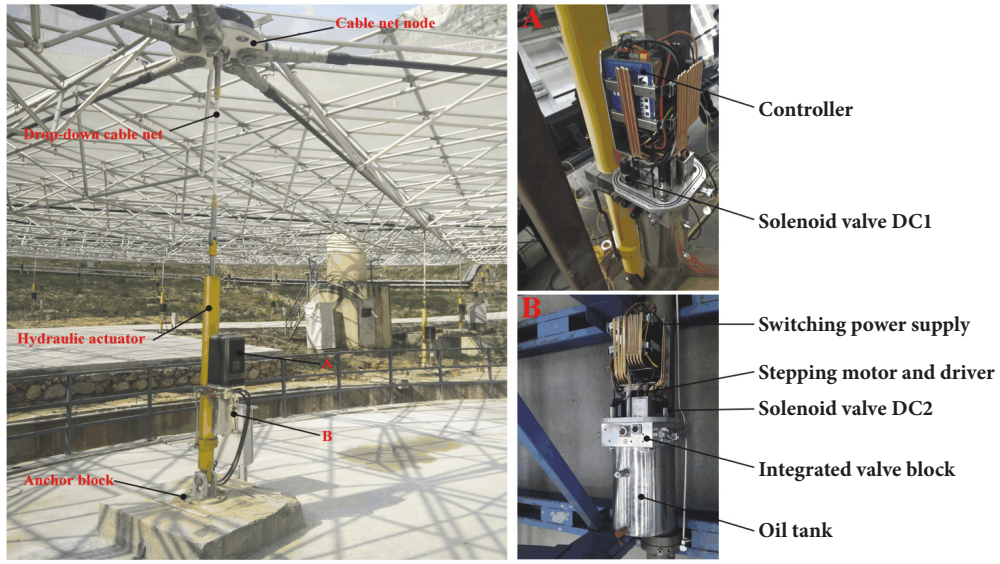

Figure 16: Field experiment.

the velocity error is about 0.33mm/s. In contrast, the velocity error controlled by SGPID strategy reduced to 0.05mm/s with no velocity oscillation.

Overall, the velocity error of PID strategy is too large, while SGPID strategy makes the velocity error remain within 0.05mm/s, which meets the requirement of FAST project.

5.2. Simulation of Scanning Tracking. In order to simulate the working condition of the active reflector system tracking the target, the switch OA in Figure 11 switched on to realize the position closed-loop control of the system. The approximate equation of the target curve is obtained by fitting the data, which can be expressed as

$$\begin{aligned} y = {} & -1.627 \times 10^4 + 1.303 \times 10^4 \cdot \cos(\omega t) + 2.098 \\ & \times 10^4 \cdot \sin(\omega t) + 4398 \cdot \cos(2\omega t) - 8900 \\ & \cdot \sin(2\omega t) - 1293 \cdot \cos(3\omega t) + 125.7 \cdot \sin(3\omega t) \\ & + 129.3 \cdot \cos(4\omega t) + 169.1 \cdot \sin(4\omega t) \end{aligned} \tag{17}$$

The target curve is shown in Figure 15(a), where $\omega = 2.11375$rad/s. Similarly, with the two control strategies applied to the hydraulic system under the same control parameters ($K_p = 50.19$, $K_i = 1.9$, and $K_d = 0.72$), the position error curve is shown in Figure 15(b).

Therefore, the position tracking error controlled by PID strategy is within 0.6mm, but SGPID control strategy can make it remain within 0.18mm, which greatly improves the tracking accuracy.

6. Experimental Study

In order to verify the working performance of the hydraulic actuator, a field experiment is carried out to compare the control effects of PID strategy and SGPID strategy, which is shown in Figure 16. The internal structure of the actuator is illustrated in subfigure A and subfigure B.

6.1. Experiment of Changing the Target Source. Velocity control of the piston rod is achieved by the velocity closed-loop control of the system, so that the piston rod realizes the point-to-point movement at speed of −1.6mm/s and

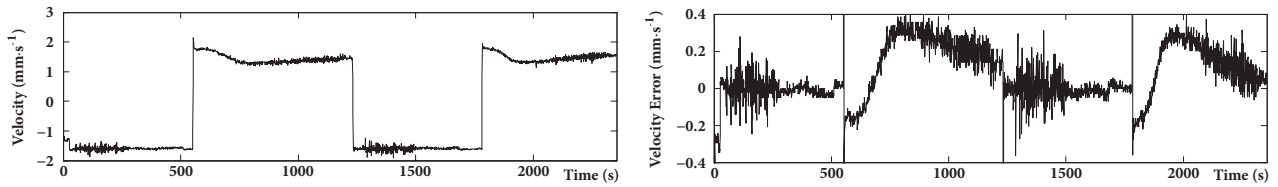

(a) (b)

Figure 17: The control effect of PID.

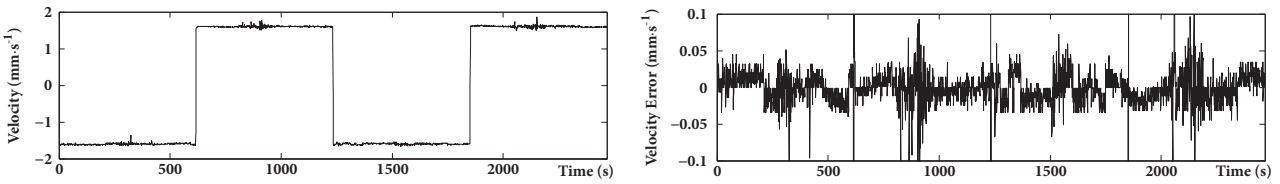

(a) (b)

Figure 18: The control effect of SGPID.

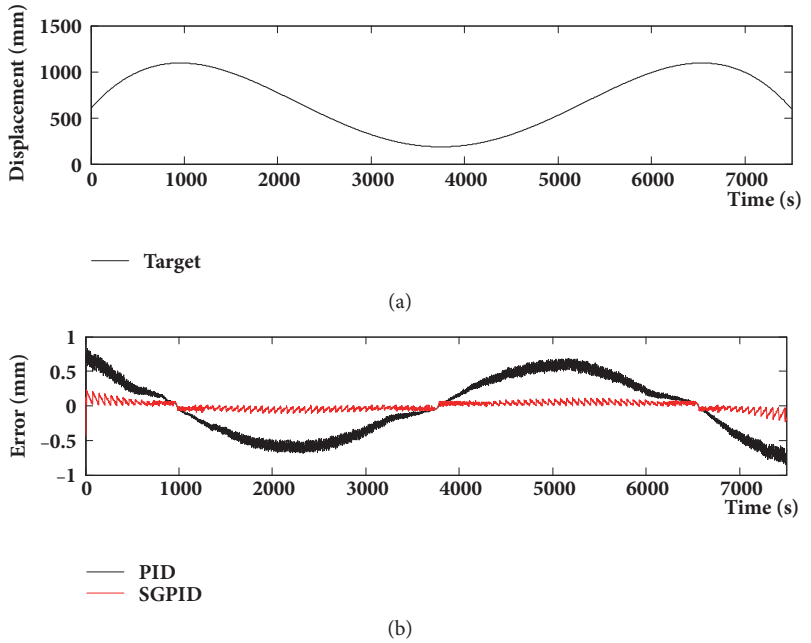

(a)

(b)

Figure 19: Experiment of the scanning tracking condition.

speed of +1.6mm/s. Figure 17 is the control effect of the hydraulic actuator under PID strategy. When the piston rod is retracted at a speed of −1.6mm/s, the velocity response is rapid, but it oscillates at the early stage; the velocity error is about 0.2mm/s. As the piston rod extends out at a speed of +1.6mm/s, the velocity appears with obvious fluctuation, oscillation, and overshoot, and the velocity error is about 0.4mm/s.

In contrast, control effect of SGPID strategy is shown in Figure 18. There is no overshoot and fluctuation; the velocity error is reduced to less than 0.05mm/s. Therefore, the experiment proved that SGPID control strategy can improve the performance of the actuator effectively.

6.2. Experiment of Scanning Tracking. The hydraulic actuator realizes scanning tracking by the position closed-loop control of the system. The experimental result of scanning tracking is shown in Figure 19. It shows that the fluctuation amplitude of the position error is large (about 0.75mm) under PID strategy, but the position error controlled by SGPID strategy is within 0.2mm, whose stability is improved significantly.

7. Conclusion

The article presents an integrated study approach about modeling, analysis, and simulation of a new closed-loop pump-controlled differential hydraulic cylinder system, which is

specially applied to the five hundred-meter aperture spherical radio telescope project.

The bond graph model of the complete system has been developed. Combining the pump-controlled differential cylinder with a motor circuit, the dynamic response of the closed-loop system is analyzed. To achieve the desired performance of the system with respect to the changing the target source condition and the scanning tracking condition, a suitable controller named SGPID is designed, whose adjustment mechanism is very convenient for engineering application. The close agreement between the experiment result and the simulation result validates the appropriateness of the proposed model and the effectiveness of adjustment mechanism of SGPID.

The results indicate that the SGPID control strategy is able to eliminate and reduce the velocity fluctuation and oscillation. Meanwhile, both the velocity error and the position error are controlled within a required range. It not only improves the dynamic performance of the hydraulic actuator, but also provides good protection for the normal work of the active reflector system.

Conflicts of Interest

The authors declare that there are no conflicts of interest regarding the publication of this paper.

Acknowledgments

This paper is supported by the *Tianjin Science and Technology Supporting Key Projects* (16YFZCGX00820). The authors wish to acknowledge the *URANUS Hydraulic Machinery Co., Ltd., China,* for providing fund in this research. Thanks are due to all the members of laboratory for providing help during the development of this research.

References

[1] R. Nan, D. Li, C. Jin et al., "The five-hundred-meter aperture spherical radio telescope (FAST) project," *International Journal of Modern Physics D*, vol. 20, no. 6, pp. 989–1024, 2011.

[2] D. Li, R. Nan, and Z. Pan, "The five-hundred-meter aperture spherical radio telescope project and its early science opportunities," *Proceedings of the International Astronomical Union: Neutron Stars and Pulsars: Challenges and Opportunities after 80 Years*, vol. 8, no. 291, pp. 325–330, 2012.

[3] X. Tang and Z. Shao, "Trajectory generation and tracking control of a multi-level hybrid support manipulator in FAST," *Mechatronics*, vol. 23, no. 8, pp. 1113–1122, 2013.

[4] J. Xiao, J. Ji, Y. Yao, B. Liu, J. Zhang, and Z. Bai, "Application of grey predictor based algorithm to hydraulic actuator used in FAST project," *Tianjin Daxue Xuebao (Ziran Kexue yu Gongcheng Jishu Ban)/Journal of Tianjin University*, vol. 49, no. 2, pp. 178–185, 2016.

[5] Ji. Jun, *Development and Performance Analysis of the Hydraulic Actuator Used in the Active Reflector System of the FAST Project, Master Thesis*, Tianjin University, Tianjin, 2016.

[6] Xin Zuo, Jian-wei Liu, Xin Wang, and Hua-qing Liang, "Adaptive PID and Model Reference Adaptive Control Switch Controller for Nonlinear Hydraulic Actuator," *Mathematical Problems in Engineering*, vol. 2017, Article ID 6970146, 15 pages, 2017.

[7] E. Kolsi-Gdoura, M. Feki, and N. Derbel, "Observer Based Robust Position Control of a Hydraulic Servo System Using Variable Structure Control," *Mathematical Problems in Engineering*, vol. 2015, Article ID 724795, 11 pages, 2015.

[8] Jianyong Yao, Guichao Yang, and Dawei Ma, "Internal Leakage Fault Detection and Tolerant Control of Single-Rod Hydraulic Actuators," *Mathematical Problems in Engineering*, vol. 2014, Article ID 345345, 14 pages, 2014.

[9] G. K. D. H. Z. C. C. Minglan, "Progress of the human-vehicle closed-loop system manoeuvrability's evaluation and optimization," *Chinese Journal of Mechanical Engineering*, vol. 39, pp. 27–35, 2003.

[10] L. Quan, F. Li, H. Tian, and Z. Yan, "Principle and application of differential cylinder system controlled with displacement pump, accumulator and proportional valve," *Jixie Gongcheng Xuebao/Chinese Journal of Mechanical Engineering*, vol. 42, no. 5, pp. 115–119, 2006.

[11] A. E. Alemu and Y. Fu, "Sliding mode control of electro-hydrostatic actuator based on extended state observer," in *Proceedings of the 29th Chinese Control and Decision Conference, CCDC 2017*, pp. 758–763, China, May 2017.

[12] Y. Lin, Y. Shi, and R. Burton, "Modeling and robust discrete-time sliding-mode control design for a fluid power electrohydraulic actuator (EHA) system," *IEEE/ASME Transactions on Mechatronics*, vol. 18, no. 1, pp. 1–10, 2013.

[13] L. Quan, "Current state, problems and the innovative solution of electro-hydraulic technology of pump controlled cylinder," *Jixie Gongcheng Xuebao/Chinese Journal of Mechanical Engineering*, vol. 44, no. 11, pp. 87–92, 2008.

[14] H. Zhao, H. Zhang, L. Quan, and B. Li, "Characteristics of asymmetrical pump controlled differential cylinder speed servo system," *Jixie Gongcheng Xuebao/Journal of Mechanical Engineering*, vol. 49, no. 22, pp. 170–176, 2013.

[15] W. Shen, Y. Pang, and J. Jiang, "Robust controller design of the integrated direct drive volume control architecture for steering systems," *ISA Transactions®*, vol. 78, pp. 116–129, 2018.

[16] H. Zhang, X. Liu, J. Wang, and H. R. Karimi, "Robust H_∞ sliding mode control with pole placement for a fluid power electrohydraulic actuator (EHA) system," *The International Journal of Advanced Manufacturing Technology*, vol. 73, no. 5-8, pp. 1095–1104, 2014.

[17] Q. Gao, L.-J. Ji, Y.-L. Hou, Z.-Z. Tong, and Y. Jin, "Modeling of electro-hydraulic position servo system of pump-controlled cylinder based on HHGA-RBFNN," in *Proceedings of the 2011 International Conference on Electronics, Communications and Control, ICECC 2011*, pp. 335–339, China, September 2011.

[18] E. Kilic, M. Dolen, H. Caliskan, A. Bugra Koku, and T. Balkan, "Pressure prediction on a variable-speed pump controlled hydraulic system using structured recurrent neural networks," *Control Engineering Practice*, vol. 26, no. 1, pp. 51–71, 2014.

[19] E. Kayacan and O. Kaynak, "Grey prediction based control of a non-linear liquid level system using PID type fuzzy controller," in *Proceedings of the 2006 IEEE International Conference on Mechatronics, ICM*, pp. 292–296, Hungary, July 2006.

[20] J. Lin, H. Chiang, and C. C. Lin, "Tuning PID control parameters for micro-piezo-stage by using grey relational analysis," *Expert Systems with Applications*, vol. 38, no. 11, pp. 13924–13932, 2011.

[21] E. Kayacan and O. Kaynak, "An adaptive grey PID-type fuzzy controller design for a non-linear liquid level system," *Transactions of the Institute of Measurement & Control*, vol. 31, no. 1, pp. 33–49, 2009.

[22] N. Yu, W. Ma, and M. Su, "Application of adaptive Grey predictor based algorithm to boiler drum level control," *Energy Conversion and Management*, vol. 47, no. 18-19, pp. 2999–3007, 2006.

[23] D. Q. Truong and K. K. Ahn, "Force control for hydraulic load simulator using self-tuning grey predictor - fuzzy PID," *Mechatronics*, vol. 19, no. 2, pp. 233–246, 2009.

[24] Xiao. Juliang, Wang. Guodong, Yan. Xiangan et al., "Switching grey prediction fuzzy control research and application," *Journal of Tianjin University*, vol. 40, no. 7, pp. 859–863, 2007.

[25] Tianjin Uranus Hydraulic Machinery Co., Ltd. "Hydraulic Actuator," China Patent No.103307059A, Sep. 18, 2013.

[26] S. Habibi, "Design of a new high-performance ElectroHydraulic Actuator," *IEEE/ASME Transactions on Mechatronics*, vol. 5, no. 2, pp. 158–164, 2000.

[27] K. K. Ahn, D. N. C. Nam, and M. Jin, "Adaptive backstepping control of an electrohydraulic actuator," *IEEE/ASME Transactions on Mechatronics*, vol. 99, pp. 1–9, 2013.

[28] G. Sun and M. Kleeberger, "Dynamic responses of hydraulic mobile crane with consideration of the drive system," *Mechanism and Machine Theory*, vol. 38, no. 12, pp. 1489–1508, 2003.

[29] K. Dasgupta, J. Watton, and S. Pan, "Open-loop dynamic performance of a servo-valve controlled motor transmission system with pump loading using steady-state characteristics," *Mechanism and Machine Theory*, vol. 41, no. 3, pp. 262–282, 2006.

[30] P. Athanasatos and T. Costopoulos, "Proactive fault finding in a 4/3-way direction control valve of a high pressure hydraulic system using the bond graph method with digital simulation," *Mechanism and Machine Theory*, vol. 50, pp. 64–89, 2012.

[31] K. Dasgupta and H. Murrenhoff, "Modelling and dynamics of a servo-valve controlled hydraulic motor by bondgraph," *Mechanism and Machine Theory*, vol. 46, no. 7, pp. 1016–1035, 2011.

[32] Shi. Jingzhuo and Zhang. Jingsong, "A two-phase hybrid stepping motor vector control servo system," *Electric Machines and Control*, vol. 4, no. 3, pp. 135–139, 2000.

[33] H.-J. Zhang, L. Quan, and B. Li, "Performance of differential cylinder position servo system controlled by permanent magnet synchronous motor driven pump," *Zhongguo Dianji Gongcheng Xuebao/Proceedings of the Chinese Society of Electrical Engineering*, vol. 30, no. 24, pp. 107–112, 2010.

[34] Deng. Julong, Wuhan: Huazhong University of Science and Technology, 1993.